Biophysical Journal Volume 101 November 2011 2082–2091

Qualitative Network Modeling of the Myc-p53 Control System of Cell Proliferation and Differentiation

Baltazar D. Aguda,[†*] Yangjin Kim,[‡] Hong Sug Kim,[†] Avner Friedman,[§] and Howard A. Fine[†¶]
[†]Neuro-Oncology Branch, Center for Cancer Research, National Cancer Institute and [¶]National Institute of Neurological Disorder and Stroke, National Institutes of Health, Bethesda, Maryland; [‡]Department of Mathematics and Statistics, University of Michigan, Dearborn, Michigan; and [§]Mathematical Biosciences Institute, The Ohio State University, Columbus, Ohio

ABSTRACT A kinetic model of a molecular control system for the cellular decision to proliferate or differentiate is formulated and analyzed for the purpose of understanding how the system can break down in cancer cells. The proposed core of this control system is composed of the transcription factors Myc and p53. The network of interactions between these factors involves negative and positive feedback loops that are linked to pathways involved in differentiation, cell cycle, and apoptosis. Understanding the dynamics of the Myc-p53 control system is aided by the postulate that there exists a cancer zone defined as a range of oncogenic Myc activities where the probability of initiating cancer is high. We propose that an essential role of p53 is to prevent the system from entering or staying too long in the cancer zone by downregulating Myc or, when Myc activity somehow becomes too high, by inducing apoptosis, cell cycle arrest, or differentiation. Kinetic modeling illustrates how deletions or aberrations in PTEN, MDM2, and ARF (genes implicated in various cancers, including glioma) affect the Myc-p53 control system. In addition, computer simulations demonstrate how this control system generates different cellular phenotypes characterized by rates of cellular differentiation and proliferation.

INTRODUCTION

Several studies point to the proto-oncogene c-Myc and the tumor suppressor gene p53 as key players in the control of stem or progenitor cell proliferation and differentiation (1,2). Perturbations in the function of either of these proteins could lead to increased cell proliferation without concomitant differentiation, resulting in a continuous supply of stem cells with tumorigenic potential (3–6). For example, deletion of p53 and PTEN in mouse neural stem cells gives rise to poorly differentiating cells with increased Myc protein levels and high proliferation rates, resulting in malignant tumors that resemble glioblastomas (7–9). In this article, we attempt to integrate and organize the Myc-p53 interactions to reveal how they coordinate cell proliferation and differentiation. We then propose and analyze a modular qualitative network model to predict cellular phenotypes characterized by degrees of differentiation, rates of proliferation and apoptosis; and we identify six phenotypes at this level of network resolution.

Myc and p53 affect cell differentiation and proliferation in opposite but nonindependent ways (see details in Table S1 in the Supporting Material). We highlight the fact that Myc and p53 interact through negative and positive feedback loops, and predicting their influence on cell proliferation and differentiation is not straightforward. We therefore formulate kinetic models to aid our understanding of the dynamics of the network. These mathematical models are phenomenological in nature because we are only representing the qualitative trend of how a change in the activity of a protein in the network affects its targets.

We illustrate how to find effective control parameters associated with the Myc-p53 feedback loops and demonstrate how perturbations of these parameters affect Myc levels. Some of these perturbations could induce Myc to enter a cancer zone (CZ) where a range of Myc levels gives significant probability of cancer initiation (the CZ postulate is described in more detail in the next section). We discuss how some of the Myc-p53 interactions may also be accomplished through indirect pathways and, as a specific example, illustrate how two of the major signaling pathways compromised in gliomas (PTEN/AKT and ARF/MDM2 pathways) are linked to the core Myc-p53 control system. Finally, we demonstrate by kinetic simulations how different cell phenotypes are generated by signaling pathways to the Myc-p53 system that controls the downstream pathways involved in cell proliferation and differentiation.

METHODS

The PubMed literature database (http://pubmed.org) was searched for genetic, biochemical, and other molecular interactions involving Myc and p53, and for their influence on proliferation and differentiation of mammalian cells (human, mouse and rat). These interactions are summarized in Fig. 1 *a*. The qualitative interactions (*arrow* and *hammerhead*) are either direct or indirect, and are given the following kinetic interpretation: $X \rightarrow Y$ means increase in X leads to a positive rate of change of Y, and $X \dashv Y$ means increase in X leads to a negative rate of change in Y (see Aguda and Goryachev (10) for more discussion of this interpretation). Table S1 lists specific interactions and literature references for the interactions depicted in Fig. 1 *a*.

As indicated in the Cell Proliferation Module in Fig. 1 *a*, proliferation is determined by the net activities of cell cycle factors (P_C) and apoptosis

Submitted August 3, 2011, and accepted for publication September 30, 2011.

*Correspondence: agudabd@mail.nih.gov or bdaguda@gmail.com

Editor: Reka Albert.

0006-3495/11/11/2082/10 $2.00

doi: 10.1016/j.bpj.2011.09.052

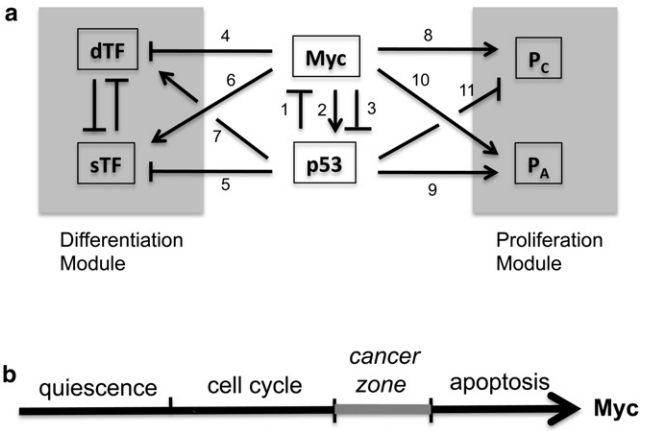

FIGURE 1 (*a*) A qualitative network involving Myc and p53 in the control of cell proliferation and differentiation. (*Arrows*) Activation or upregulation. (*Hammerheads*) Inhibition or downregulation. Table S1 in the Supporting Material lists references supporting interactions 1–11. Abbreviations: *sTF*, stemness transcription factors; *dTF*, transcription factors inducing differentiation; P_C, cell cycle factors; P_A, apoptosis factors. (*b*) As Myc activity increases, a cell transitions from quiescence to the cell cycle, and eventually to apoptosis. The cancer zone is postulated to exist between normal cell cycle and apoptosis.

factors (P_A). Similarly, as shown in the Differentiation Module, cell differentiation occurs when the activities of differentiation transcription factors (dTF) dominate those of stemness transcription factors (sTF). Examples of sTF are the pluripotency factors Oct4, Sox2, and Nanog (11,12). Examples of dTF are transcription regulators such as GATA6 and CDX2 that induce the endoderm and trophectoderm lineages, respectively (13). Cellular phenotypes are characterized according to the relative activities of the four submodules P_C, P_A, sTF, and dTF. Kinetic modeling of the detailed networks of these submodules are interesting problems in their own right (13–17), but will not be considered in detail here.

We refer to the interactions represented by edges 1–3 in Fig. 1 *a* as the core Myc-p53 control system. The dynamics of this system is modeled by a system of ordinary differential equations according to the aforementioned kinetic interpretation of arrows and hammerheads in the model network. These equations are then recast into dimensionless forms to reduce the number of parameters and determine the effective control parameters. The control parameters associated with the feedback loops between Myc and p53 are perturbed to investigate the sensitivity of Myc on these parameters. To interpret the significance of the magnitudes of the changes in Myc, we invoke the existence of a cancer zone (CZ) defined as a range of Myc activities wherein the probabilities of initiating cancer are high. The CZ postulate was first proposed by Aguda et al. (18) and is in strong accord with the experimental observations in vivo (e.g., see Murphy et al. (19) and Aguda and Algar (14)). As illustrated in Fig. 1 *b*, a cell transitions through states of quiescence, cell cycling, and apoptosis as Myc activity increases; in between cell cycling and apoptosis is the postulated CZ.

Myc and p53 are coupled to two of the major deregulated signaling pathways involved in gliomagenesis, namely, the ARF/MDM2 and PTEN/AKT pathways (20). The Myc-p53 network is extended with simplified versions of these pathways, and a correspondingly extended system of dimensionless differential equations is used to describe the dynamics of the composite network. Because they are common perturbations in gliomas, the effects of deleting the genes PTEN and ARF, and the overexpression of MDM2, on the levels of Myc are simulated.

The final set of model differential equations studied in this article involves the core Myc-p53 control system and signaling pathways to the Differentiation Module and Proliferation Module (these modules' components are shown in Fig. 1 *a*). To illustrate how various cellular phenotypes are generated by this modular network, we varied the strengths of two signaling pathways, one to Myc and the other to dTF.

All model differential equations are computationally integrated using routine ode23 in MATLAB (The MathWorks, Natick, MA). Values of dimensionless parameters are estimated from published experimental values where available. For example, the following values of protein half-lives ($t_{1/2}$) are used: Myc, ~20–30 min (21); p53, ~15 min (22); Mdm2, ~30 min (23); Pten, >12 h (24); and ARF, ~6 h (25). A first-order protein decay coefficient (d) is related to the half-life by the formula $d = (ln\ 2)/t_{1/2}$. Dimensionless kinetic equations generally require only knowledge of ratios of parameters (i.e., not their absolute values). The arbitrarily assigned values for some of the dimensionless parameters in our simulations may be considered as predictions on the ratios of the absolute values of corresponding parameters that generate the dynamic behavior exhibited by the models.

RESULTS AND DISCUSSION

Failsafe mechanisms of the Myc-p53 control system and possible cell phenotypes

When proliferative signals increase Myc activity, cells are induced to enter the cell cycle as indicated by edge 8 in Fig. 1 *a*. Increases in Myc are attenuated by the negative feedback loop composed of edges 1 and 2. If this attenuation fails and Myc increases out of control, several failsafe mechanisms are available to negate Myc's oncogenic potential. These mechanisms include p53-dependent (edges 2 and 9) and p53-independent (edge 10) cell death via apoptosis, p53-dependent cell cycle arrest (edge 11), and p53-induced cell differentiation (edges 5 and 7). Which of these failsafe mechanisms are operative would depend on the parameters and initial conditions of the system. Note that edge 3 forms a loop of mutual repression between Myc and p53 (a positive feedback loop) that compromises the aforementioned p53-mediated failsafe mechanisms.

A qualitative analysis of the modular model in Fig. 1 *a* suggests how various cellular phenotypes can be generated. Let the right superscripts "+" and "−" on a submodule mean "on" and "off," respectively. Inside the Differentiation Module, two combinations of the submodule states are probable, namely, $[sTF]^+[dTF]^-$ and $[sTF]^-[dTF]^+$, because of the mutual antagonism between sTF and dTF. Let $D^+ = [sTF]^-[dTF]^+$ and $D^- = [sTF]^+[dTF]^-$ represent differentiating and undifferentiated cells, respectively. Inside the Proliferation Module, three combinations of the submodule states are possible, namely, C^+A^-, C^-A^+, and C^-A^-, where C and A are associated with the P_C and P_A submodules, respectively, as shown in Fig. 1 *a*. There are six possible submodule combinations and phenotypes as listed in the first and second columns, respectively, of Table 1. The third column lists the possible values of Myc, namely, m_Q (set of values of Myc for quiescent cells), m_C (set of values of Myc for cells in the cell cycle), m_{CZ} (set of values of Myc for cells in the cancer zone), and m_A (set of values of Myc for cells undergoing apoptosis).

TABLE 1 Six cellular phenotypes and corresponding qualitative values of Myc

Submodule combinations	Cellular phenotypes	Values of Myc (m)
D+C+A−	Differentiating proliferating cells (cancer transit-amplifying cells possible)	$m \in \{m_C, m_{CZ}\}$
D+C−A+	Dying differentiated quiescent cells	$m \in m_A$
D+C−A−	Differentiated quiescent cells	$m \in m_Q$ or $m \in \{m_C, m_{CZ}\}$ but cell-cycle arrested cells
D−C+A−	Undifferentiated dividing cells (cancer-stem-like cells possible)	$m \in \{m_C, m_{CZ}\}$
D−C−A+	Dying undifferentiated quiescent cells (dying normal stem cells)	$m \in m_A$
D−C−A−	Undifferentiated quiescent cells (normal stem cells)	$m \in m_Q$ or $m \in \{m_C, m_{CZ}\}$ but cell-cycle arrested cells

Controlling the feedback loops between Myc and p53

The core Myc-p53 network and its associated generalized dynamical equations are shown in Fig. 2. Signaling pathways to Myc and p53 are indicated by s_1 and s_2, respectively, and protein degradation pathways are shown with rate coefficients δ_m and δ_p. By nondimensionalizing the equations, we show here that the parameters of the network can be lumped into a fewer number of effective control parameters.

The variables m and p in the phenomenological equations in Fig. 2 *b* are protein activities of Myc and p53, respectively. As indicated in the *b1* equation in the figure, the signal s_1 increases the rate of Myc activation through the function $f(s_1)$, whereas p53-dependent inhibition of Myc is through the function $F(p)$ in the denominator. A requirement on these functions is that $\partial f/\partial s_1 \geq 0$ for all nonnegative s_1, and $\partial F/\partial p \geq 0$ for all nonnegative p. Similarly, the second term on the right-hand side of the *b2* equation in the figure represents the increase in p53 activity induced by signal s_2, and Myc-dependent suppression of p53 activity through the function $H(m)$ in the denominator. Myc-dependent increase in p53 activity is represented by the function $g(m)$. One must also have $\partial H/\partial m \geq 0$ and $\partial g/\partial m \geq 0$ for all nonnegative m.

Consider a simple case where $f(s_1) = s_1$, $g(m) = m$, $h(s_2) = s_2$, $F(p) = p$, and $H(m) = m$ so that the dynamical equations are

$$\frac{dm}{dt} = \frac{\varepsilon_1 s_1}{k_1 + p} - \delta_m m, \tag{1}$$

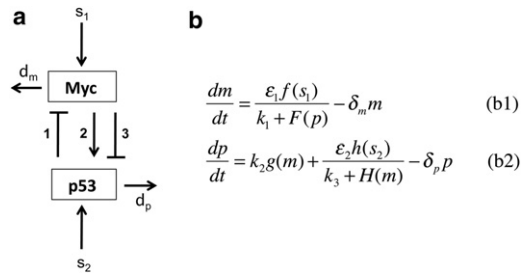

FIGURE 2 (*a*) The Myc-p53 core control system, and its (*b*) generalized phenomenological dynamical equations. See text for details.

$$\frac{dp}{dt} = k_2 m + \frac{\varepsilon_2 s_2}{k_3 + m} - \delta_p p. \tag{2}$$

These equations can be recast in dimensionless forms as follows:

$$\frac{dm^*}{dt^*} = \frac{1}{k_1' + s_2' p^*} - m^*, \tag{3}$$

$$\delta' \frac{dp^*}{dt^*} = k_2' m^* + \frac{1}{k_3' + s_1' m^*} - p^*, \tag{4}$$

where

$$t^* = \delta_m t,\ m^* = \frac{m}{s_1},\ p^* = \frac{p}{s_2}, \tag{5}$$

$$k_1' = \frac{\delta_m}{\varepsilon_1} k_1,\ k_2' = \frac{s_1}{s_2 \delta_p} k_2,\ k_3' = \frac{\delta_p}{\varepsilon_2} k_3, \tag{6}$$

$$s_1' = \frac{\delta_p}{\varepsilon_2} s_1,\ s_2' = \frac{\delta_m}{\varepsilon_1} s_2,\ \delta' = \frac{\delta_m}{\delta_p}. \tag{7}$$

The dimensionless parameters in Eqs. 3 and 4 are referred to as effective control parameters. For example, the strength of the inhibition of Myc by p53 can be controlled through the dimensionless parameter s_2' that, according to the middle expression in Eq. 7, is directly proportional to the parameter of the signaling pathway to p53 (s_2), directly proportional to the parameter for the degradation of Myc (δ_m), and inversely proportional to the coefficient of signaling to Myc (ε_1). Varying the parameters s_2, δ_m, and ε_1 in different ways but keeping the same value of s_2' will generate qualitatively identical behaviors. To represent a mutation in p53 that would decrease its ability to downregulate Myc activity, one could decrease the value of k_1' or s_2'. For instance, a deletion of p53—corresponding to setting s_2' to 0—could explain the observed increased Myc levels in neural stem cells of p53-knockout mice (7). Another interesting example of an effective control parameter is k_2', which is associated with Myc-dependent activation of p53. According to the middle expression in Eq. 6, to increase k_2', one can increase

either k_2 or s_1, or decrease s_2 (signal to p53) or the degradation rate of p53 (δ_p).

Computer simulations using Eqs. 3 and 4 are shown in Fig. 3. Due to the negative feedback between Myc and p53, and with the chosen initial conditions (given in the legend of Fig. 3 *a*), Myc spikes and decreases as p53 builds up. For illustrative purposes only, the cancer zone (CZ) is arbitrarily represented by the shaded band in Fig. 3 (between $m^* = 3$ and $m^* = 4.5$). We propose that the amount of time spent inside the CZ (as indicated by the dark-shaded area, A_{CZ}, in Fig. 3 *a*) is a key determinant of the probability of initiating carcinogenesis. The larger the A_{CZ}, the greater this probability. Note that even if Myc enters CZ, the probability could be negligible if the time spent in CZ is insignificant. Long-term elevated levels of Myc within CZ, as exemplified by Fig. 3, *c* and *d*, give rise to significant probabilities of initiation of cancer.

In the simulations shown in Fig. 3, *b–d*, we illustrate how Myc enters or exits CZ when the strength of the negative feedback loop between Myc and p53 varies—e.g., as the values of k_2' or s_2' change. Increasing either k_2' or s_2' lowers Myc long-term (steady state) activity, thereby pushing the system below the CZ (Fig. 3, *b* and *c*). In contrast, increasing s_1' strengthens the positive feedback loop between Myc and p53, driving entry into the CZ. Note that the values of k_2' and s_1' relative to each other determine whether the negative feedback between Myc and p53 (edges 1 and 2 in Fig. 1 *a*) is stronger or weaker than the positive feedback between these factors (edges 1 and 3). Increasing s_1' and decreasing s_2' favors Myc in its battle against p53. When manipulating the parameters k_2', s_2', and s_1', we emphasize that the expressions of the dimensionless parameters in Eqs. 6 and 7 provide key information on what parameters can be controlled experimentally.

A detailed analysis of the stability of the steady states of the core Myc-p53 system (Eqs. 3 and 4) is provided in the second part of the Supporting Material. We show that there is at most one nonnegative steady state of the system for every set of positive parameters and, importantly, a rapid increase in the steady state of Myc (m_s*) at a bifurcation point where an instability emerges. This bifurcation point is shown in Fig. 4. The bifurcation diagram looks like a pitchfork, but broken into two pieces. The parameter s_1' is the parameter associated with edge 3 in Fig. 1 *a* and is a parameter that can control the strength of the positive feedback loop (mutual antagonism) between Myc and p53. The bifurcation point is located at $s_1' \sim 0.9$, corresponding to the point where the dashed curve (unstable steady states) and the solid curve (stable steady states) merge in Fig. 4. Note that the lower broken piece of the pitchfork is in the negative region (*shaded area*). Although the saddle-node bifurcation value of m_s* is located in the negative region, this bifurcation phenomenon is manifested in the rapid increase in the positive m_s* immediately to the right of the bifurcation point. Details in the derivation of the exact conditions on the parameters for instability to occur, including the interplay between stabilizing and destabilizing loops in the network, are given in the second part of the Supporting Material. The main result is the following: an instability arises when

$$C_2^+ > C_1^m C_1^p + C_2^- \tag{8}$$

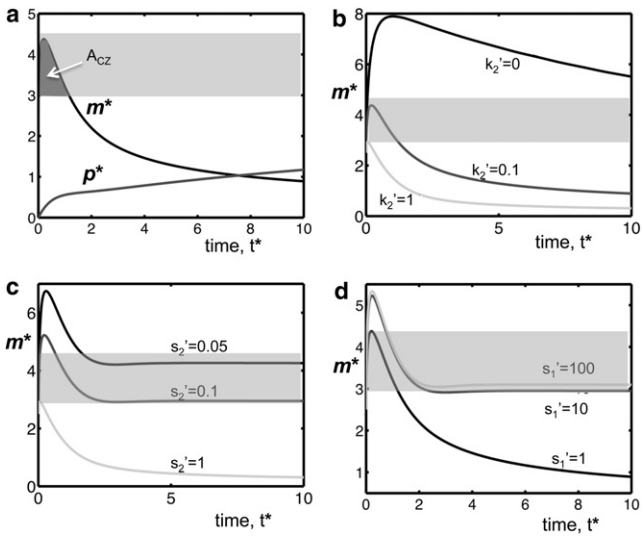

FIGURE 3 Myc and p53 activities as functions of time according to Eqs. 3 and 4. (*a*) Activities of Myc (m^*) and p53 (p^*) versus time. For illustrative purposes only, a cancer zone (CZ) is arbitrarily indicated by the gray band between $m^* = 3$ and 4.5. (*b*) Myc versus time, for varying k_2'. (*c*) Myc versus time, for varying s_2'. (*d*) Myc versus time, for varying s_1'. Parameter values: $k_1' = 0.01$, $k_2' = 0.1$ (varies in *b*), $k_3' = 0.01$, $s_1' = 1$ (varies in *d*), $s_2' = 1$ (varies in *c*), $d' = 0.5$. Initial conditions: $m^*(0) = 0.1$, $p^*(0) = 0.05$.

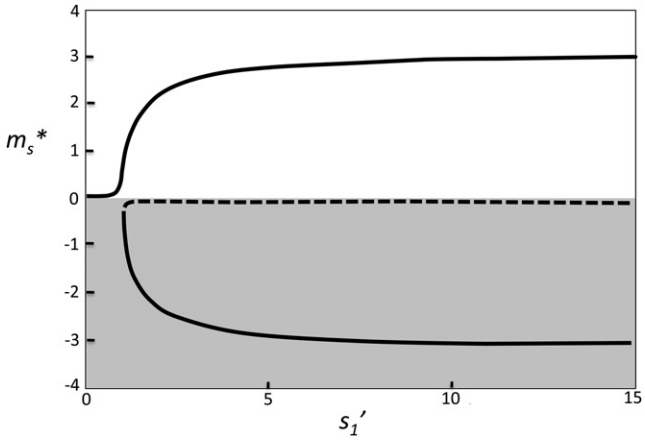

FIGURE 4 Steady state of Myc (m_s*, dimensionless) versus s_1' determined from Eqs. 3 and 4. The parameter s_1' is associated with edge 3 in Fig. 1 *a*. Negative steady states (*lower curve*, both *solid* and *dashed portions*) are in the shaded region, and are unphysical. (*Solid curves*) Stable steady states; (*dashed curve*) unstable steady states. Parameter values: $k_1' = 0.01$, $k_2' = 1$, $k_3' = 0.01$, $s_2' = 1$, and s_1' varies through the range of the abscissa in this figure.

where

$$C_2^+ = s_1' \frac{s_2' m_s^{*2}}{\delta' \left(k_3' + s_1' m_s^*\right)^2},$$
$$C_2^- = k_2' \frac{s_2' m_s^{*2}}{\delta'}, \quad (9)$$
$$C_1^m = 1 \text{ and } C_1^p = \frac{1}{\delta'}.$$

C_2^+ is a measure of the strength of the positive feedback loop (edges 1 and 3 in Fig. 1 *a*), C_2^- is that of the negative feedback loop (edges 1 and 2), and C_1^m and C_1^p are the one-cycles associated with the first-order decay of Myc and p53, respectively. Lastly, we also prove that Eqs. 3 and 4 do not give rise to periodic oscillations for all sets of positive parameters.

Perturbations of the Myc-p53 control system by PTEN, MDM2, and ARF

PTEN is a tumor suppressor gene deleted in many human cancers, including 70% of human glioblastomas (26–29). Simultaneous inactivation of p53 and PTEN in mice gives rise to undifferentiated cells with high proliferative rates and increased Myc protein levels (7). Furthermore, knocking out p53 and PTEN in mouse neural stem cells is sufficient to produce infiltrative gliomas (8).

The qualitative network shown in Fig. 5 *a* summarizes the mutually antagonistic pathways between p53 and Akt (30–32). This mutual inhibition has been proposed as a potential switching mechanism for the cellular decision to survive or die (31,33). Akt is a survival factor because it upregulates pathways inhibiting apoptosis and pathways inducing the cell cycle, whereas p53 promotes apoptosis and suppresses the cell cycle.

One could discern from Fig. 5 *a* several reasons why PTEN deletion has a significant impact on p53 activity:

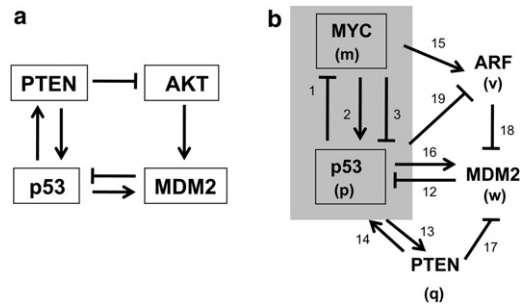

FIGURE 5 (*a*) Mutual antagonism between {p53, PTEN} and {AKT, MDM2}. (*Arrows*) Activation or upregulation. (*Hammerheads*) Inhibition or downregulation. (*b*) The Myc-p53 control system (edges 1–3) and its interactions with Pten, Mdm2, and Arf. Signaling pathways and degradation reactions are not shown.

First, PTEN helps p53 suppress the cell cycle via the pathway {*p53* → *PTEN*–|*AKT* → *cell cycle*}; in other words, loss of PTEN means cutting off the control of p53 in suppressing cell proliferation via this pathway. Second, due to the pathway {*PTEN*–|*AKT* → *MDM2*–|*p53*}, loss of PTEN implies increased MDM2-induced degradation of p53. This is why PTEN has been described as protective of p53 (34). Third, as depicted by the arrow from PTEN to p53 in Fig. 5 *a*, PTEN increases p53 stability through phosphatase-independent mechanisms (35,36).

As shown in Fig. 5 *b*, pathways involving Mdm2 and Arf also impinge on the Myc-p53 control system. Mdm2 is an oncogene frequently overexpressed in human primary glioblastomas (27,37). Mdm2 protein possesses ubiquitin ligase activity that induces degradation of p53 (38) whereas, at the transcriptional level, p53 promotes expression of Mdm2—thus, forming a negative feedback loop between these two proteins (39).

The INK4A/ARF locus is frequently deleted in human gliomas (27). Uhrbom et al. (40) first reported that loss of ARF in combination with KRas signaling generate glioblastomas in mice. More recently, Robinson et al. (41) demonstrated that a combination of activated MEK (a member of the map kinase pathway) with either activated Akt or loss of Ink4a/Arf is sufficient to transform mouse neural progenitor cells into gliomas in vivo. Zindy et al. (42) first showed that Myc signals through Arf to regulate p53-dependent apoptosis, and later gave evidence that this Arf-Mdm2-p53 tumor suppressor pathway is inactivated in certain cancers (43). As represented by edge 19 in Fig. 5 *b*, the inhibition of Arf transcription by p53 (44) completes a negative feedback loop between Arf and p53 along with edges 18 and 12. In terms of coordinating self-renewal and differentiation of mouse neural stem cells, Nagao et al. (2) observed that low levels of Arf expression promotes stem cell self-renewal, whereas overexpression of Arf induces precocious differentiation (in this case, gliogenesis)—consistent with the effects mediated by edges 18 and 12 of Fig. 5 *b* on the Arf-Mdm2-p53 pathway.

To simplify the mathematical model, we collapsed the pathway {*PTEN*–| *AKT* → *MDM2*} into a single interaction between PTEN and MDM2 (edge 17 in Fig. 5 *b*). The dynamics of this network can be described by the following set of equations (Fig. 5 *b* gives the meaning of the letters *m, p, w, q*, and *v*):

$$\frac{dm}{dt} = \frac{\varepsilon_1 s_1}{k_1 + p} - \delta_m m, \quad (10)$$

$$\frac{dp}{dt} = k_2 m + k_{14} q + \frac{\varepsilon_2 s_2}{k_3 + m + k_{12} w} - \delta_p p, \quad (11)$$

$$\frac{dw}{dt} = k_{16} p + \frac{\varepsilon_4 s_4}{k_{17} + q + k_{18} v} - \delta_w w, \quad (12)$$

$$\frac{dq}{dt} = \varepsilon_3 s_3 + k_{13}p - \delta_q q, \tag{13}$$

$$\frac{dv}{dt} = \varepsilon_5 s_5 + \frac{k_{15}m}{k_{19}+p} - \delta_v v. \tag{14}$$

Note that the indirect effect of Akt signaling is represented by the parameter s_4 in Eq. 12. The dimensionless equations corresponding to Eqs. 10–14 are given by Eqs. A1–A5, with dimensionless parameters in Eqs. A6–A10, in the Appendix.

Using Eqs. A1–A5, the effects on Myc of perturbing Pten, Arf, and Mdm2 are shown in Fig. 6. Deletion of Pten and/or Arf, as well as overexpression of Mdm2, increases the Myc steady state. The perturbations of the parameters s_3', s_4', and s_5' (Fig. 6) may also be interpreted as perturbations of signaling pathways impinging on Pten, Mdm2, and Arf, respectively (see dimensionless parameters in Eqs. A6–A10). The magnitudes of the increases in the steady state of Myc will be critical in deciding whether or not the system enters the CZ. Although experimentally measured rate parameters are not available at this time, some of the potential dynamics of the network can be predicted based on the presence of feedback loops in the network structure. The negative feedback loop between p53 and Mdm2 has been predicted—and later validated experimentally—to give rise to oscillations (33,45). Another negative feedback loop with potential to cause oscillations is formed between Arf and p53 through edges 19, 18, and 12 in Fig. 5 *b*, although no report of observation of such oscillations has been published so far. Finally, as already mentioned above (Fig. 5 *a*), the mutual antagonism between {p53, Pten} and {Akt, Mdm2} has been previously modeled and predicted to generate bistable switching behavior—i.e., an all-or-none switch between p53 and Akt (31).

Coordination of cell differentiation and proliferation by signaling pathways

To demonstrate how the various cell phenotypes (column 1 of Table 1) are generated, we formulate a dynamical model that uses Eqs. 3 and 4 for the core Myc-p53 control system, and additional equations for the submodules of cell differentiation and proliferation. We assume that there is a particular marker for sTF, dTF, P_C, and P_A, with the following symbols used for their activities: [sTF marker] = D_s, [dTF marker] = D_d, [P_C] = P_c, and [P_A] = P_a. We further assume that these markers possess specific threshold values for becoming active in driving their corresponding cellular processes; for example, when D_d surpasses a threshold θ_d, differentiation occurs. The additional equations are as follows:

$$\frac{dD_s}{dt} = \varepsilon_s s_s + \frac{(k_6 + k_{6b}m)D_s^4}{\theta_s^4 + D_s^4 + k_5 p + k_{5b}D_d} - \delta_s D_s, \tag{15}$$

$$\frac{dD_d}{dt} = \varepsilon_d s_d + \frac{(k_7 + k_{7b}p)D_d^4}{\theta_d^4 + D_d^4 + k_4 m + k_{4b}D_s} - \delta_d D_d, \tag{16}$$

$$\frac{dP_c}{dt} = \varepsilon_c s_c + \frac{(k_8 + k_{8b}m)P_c^2}{\theta_c^2 + P_c^2 + k_{11}p} - \delta_c P_c, \tag{17}$$

$$\frac{dP_a}{dt} = \varepsilon_a s_a + \frac{(k_{10} + k_{10b}m + k_9 p)P_a^2}{\theta_a^2 + P_a^2} - \delta_a P_a. \tag{18}$$

The exponents for D_s, D_d, P_c, and P_a are used to represent sigmoidal threshold kinetics where the thresholds are given by the θ-values in the denominators (the exponents for D_s and D_d are arbitrarily assumed larger than those of P_c and P_a because of the mutual repression of sTF and dTF factors—as depicted in Fig. 1 *a*—that may generate sharper switching behavior than that of proliferation or apoptosis). The dimensionless versions of Eqs. 15–18 are given by Eqs. A11–A14, with dimensionless parameters in Eqs. A15–A20, in the Appendix.

The strengths of signaling pathways are represented by six parameters, namely, s_1', s_2', s_s', s_d', s_c', and s_a' (these are the dimensionless parameters given in Eq. A19 in the Appendix). We study how two of these signaling pathways—namely, s_1' and s_d'—coordinate cell proliferation

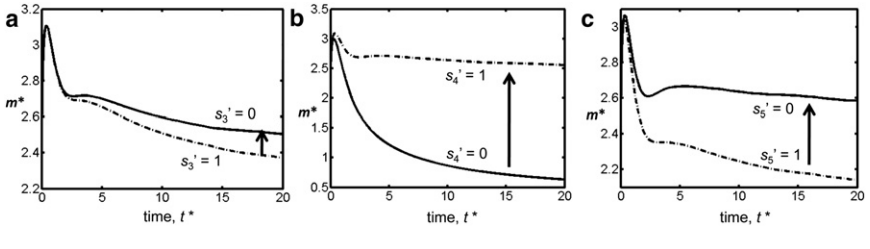

FIGURE 6 Increases in the steady state of Myc by deletion of Pten, overexpression of Mdm2, and deletion of Arf. Dimensionless Eqs. A1–A5 and parameter Eqs. A6–A10 in the Appendix are used in these simulations. (*a*) Deleting Pten (by setting $k_{14}' = s_3' = 0$) increases the steady state of Myc. Initial $q^*(0) = 0$. Parameters: $s_3' = 0$ and 1, $s_4' = 0.5$, $s_5' = 0.5$, and $k_{14}' = 0$. Other parameter values and initial conditions are listed at the bottom of this caption. (*b*) Overexpressing Mdm2 (by increasing s_4' from 0 to 1) increases the steady state of Myc. Initial $q^*(0) = 0.05$. Parameters: $s_4' = 0$ and 1, $s_3' = 1$, $s_5' = 0.5$, and $k_{14}' = 0.01$. Other parameter values and initial conditions are listed at the bottom of this caption. (*c*) Deleting Arf (by setting $s_5' = 0$) increases the steady state of Myc. Initial $q^*(0) = 0.05$. Parameters: $s_5' = 0$ and 1, $s_4' = 0.5$, $s_3' = 1$, and $k_{14}' = 0.01$. Other parameter values and initial conditions are listed below. Other parameter values: $k_1' = 0.01$, $k_2' = 0.1$, $k_3' = 0.01$, $k_{13}' = 0.01$, $k_{15}' = 0.02$, $k_{16}' = 0.02$, $k_{17}' = 0.01$, $k_{19}' = 0.01$, $s_1' = 1$, $s_2' = 1$, $e_3' = 0.1$, $e_5' = 0.1$, $d' = 0.5$, $d'' = 1$, $d''' = 30$, and $d'''' = 12$. Other initial conditions: $m^*(0) = 2.5$, $p^*(0) = 0.1$, $w^*(0) = 0.03$, and $v^*(0) = 0.05$.

and differentiation. Mitogenic signaling pathways to Myc (associated with the parameter s_1') are activated for cells to enter the cell cycle or to promote pluripotency. An example is LIF signaling, which is important in maintaining expression of Myc in mouse embryonic stem cells (46), and another is Wnt signaling (47,48). Signaling pathways that induce differentiation are represented collectively by s_d'. An example is signaling to GATA-6 (49), an endoderm master gene regulator repressed by both Myc and Nanog (50,51).

We explored the effects of varying s_1' and s_d' to demonstrate how the phenotypes listed in Table 1 can be generated by the model equations. Only four of the six phenotypes are simulated because we do not consider phenotypes with A^+ (i.e., we ignore dying cells). Equations 3 and 4 and A11–A14 are integrated until all the variables reach their steady states. Increasing s_d' leads to a switch to the D^+ phenotype, with fixed low s_1' values (associated with low Myc steady states) giving rise to terminally differentiated cells (D^+C^- in Fig. 7 *a*) and relatively higher values of s_1' (associated with high Myc steady states) to transit-amplifying cells (D^+C^+ in Fig. 7 *c*). On the other hand, for fixed values of s_d', increasing s_1' (associated with increasing Myc steady states) de-differentiate cells into the cancer stemlike phenotype (D^-C^+ in Fig. 7 *b*).

This D^-C^+ phenotype can be induced to differentiate, i.e., as transit-amplifying cells (D^+C^+), by increasing s_d' as shown in Fig. 7 *c*. In Fig. 7 *d*, we show the locations of these four phenotypes on a phase diagram with coordinates s_1' and s_d'. This is a low-resolution phase diagram because we arbitrarily assigned high thresholds for the steady states $D_d{}^{*s}$ (to distinguish D^+ from D^-) and $P_c{}^{*s}$ (to distinguish C^+ from C^-). As illustrated in Fig. 7 *d*, there are regions where different phenotypes can be generated despite all the model parameters being fixed. For example, the shaded area with corners *a*, *b*, *c*, and *d* in Fig. 7 *d* switches from D^+C^- to D^+C^+ if the initial conditions for $D_d{}^*$ and $P_c{}^*$ are increased (the figure caption gives values of this change); concomitantly, the darker-shaded area with corners *b*, *c*, *e*, and *f* in Fig. 7 *d* switches from D^-C^- to D^-C^+. Thus, both the strengths of the signaling pathways (s_1' and s_d') and the initial conditions of the system are important in deciding which phenotype is obtained.

CONCLUSIONS

Two recent census of human cancer genes list Myc and p53 in the top groups of frequently amplified and mutated genes, respectively (52,53). As transcription factors, Myc has been estimated to bind 10–15% of all gene promoters in the human genome (54,55), and, for p53, nearly 5000 genes have at least one p53 consensus binding sequence in their promoter regions (56,57). It is therefore not surprising that these factors have been shown in many instances to play key roles in stem/progenitor cell proliferation and differentiation. We have reviewed the literature and summarized the evidence showing that Myc and p53 exert opposite effects on these cellular processes (Fig. 1 *a* and see Table S1). Because proliferation and differentiation are not independent processes in a developing organism, we expect that Myc and p53 must talk to each other. Indeed, such a bidirectional communication exists as illustrated by the negative feedback loop between edges 1 and 2 in Fig. 1 *a*.

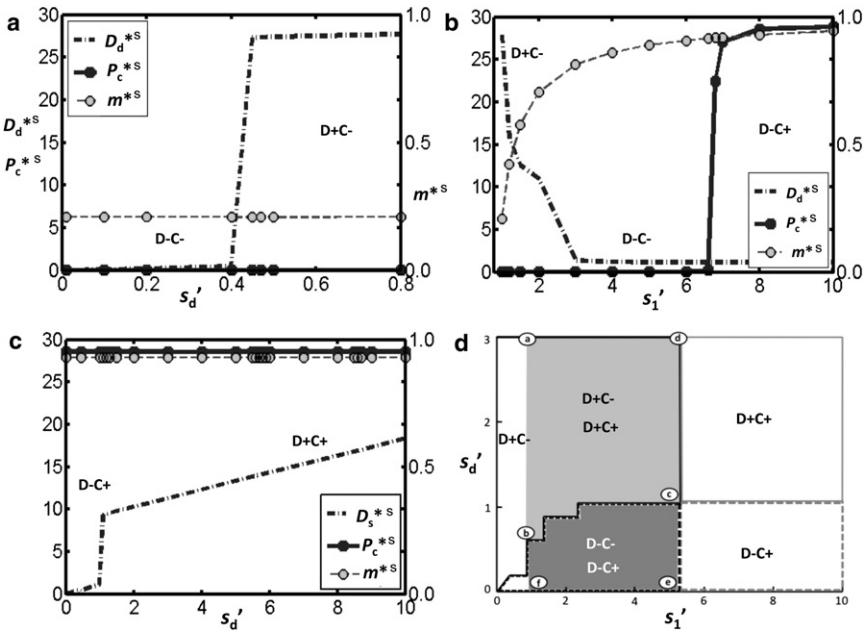

FIGURE 7 Steady states $D_d{}^{*s}$, $P_c{}^{*s}$, and m^{*s} versus signaling parameters s_1' and s_d' (*a*) for varying s_d' with $s_1' = 1$, (*b*) for varying s_1' with $s_d' = 1$, and (*c*) for varying s_d' with $s_1' = 8$. (*d*) Phase diagram showing the location of the phenotypes, with D^+ assigned for $D_d{}^{*s} \geq 10$ and D^- otherwise, and C^+ assigned for $P_c{}^{*s} \geq 10$ and C^- otherwise. For the initial conditions given below, the rightmost boundary between D^+C^- and D^+C^+ is given by the line segment *cd*; this boundary shifts to the line segment *ab* when the initial conditions $D_d{}^*(0)$ and $P_c{}^*(0)$ are increased to 1 and 0.1, respectively (other initial conditions fixed as given below). This change in initial conditions also shifts the boundary between D^-C^- and D^-C^+ from line segments *ce* to *bf*. Equations 3 and 4 and Eqs. A11–A14 in the Appendix are used in the simulations. Parameter values: $k_1' = 0.01$, $k_2' = 1$, $k_3' = 0.01$, $k_4' = 100$, $k_{4b}' = 0.1$, $k_5' = 0.1$, $k_{5b}' = 1$, $k_6' = 2.1$, $k_{6b}' = 1.6$, $k_7' = 3$, $k_{7b}' = 5$, $k_8' = 10$, $k_{8b}' = 20$, $k_9' = 1$, $k_{10}' = 1$, $k_{10b}' = 1$, $k_{11}' = 0.1$, $s_2' = 1$, $s_s' = 0.01$, $s_c' = 0.01$, $s_a' = 0.01$, $d' = 0.5$, $d_{ms}' = 2.5$, $d_{md}' = 2.5$, $d_{mc}' = 2.5$, and $d_{ma}' = 2.5$. Initial conditions: $m^*(0) = 0.1$, $p^*(0) = 0.05$, $D_s{}^*(0) = 1.1$, $D_d{}^*(0) = 0.0001$, $P_c{}^*(0) = 0.001$, and $P_a{}^*(0) = 0.0001$.

The significance of the dysregulation of this feedback loop in cancer has been suggested by Rochlitz et al. (1) more than 15 years ago. Here, we have demonstrated by kinetic modeling that decreasing the strength of this negative loop (by varying the values of the associated control parameters) leads to an increase in the peak value and/or steady state of Myc (Fig. 3, *b* and *c*). This could arise, for example, through mutation or inactivation of p53 that decreases its ability to inhibit Myc. In addition to the negative feedback loop, a direct or indirect pathway from Myc to p53 that has a net effect of inhibiting p53 would create a positive feedback loop that can cause large increases in Myc.

In terms of cancer development, the consequences of increasing Myc levels can be predicted if we can locate the cancer zone, CZ (18)—the range of Myc associated with increased probability of cancer as depicted in Fig. 1 *b*. The residence time and Myc levels (A_{CZ} in Fig. 3 *a*) within the CZ are predicted to be key factors for inducing downstream tumorigenic events. An experimental surrogate for the magnitude of A_{CZ} would be useful for predicting susceptibility to cancer.

We view the ARF/MDM2 and PTEN/AKT pathways as perturbations of the core Myc-p53 control system and, aided by kinetic modeling, have explained published reports on the effects of deletions of p53, PTEN, ARF, and overexpression of MDM2, on the phenotypes of mouse neural stem cells—thus, suggesting potential mechanisms for gliomagenesis. Furthermore, the qualitative modular network (Fig. 1 *a*) that models the coordination of cell proliferation and differentiation by the Myc-p53 control system predicts six cellular phenotypes (Table 1) and that two of these are probable cancer precursors (D^+C^+ and D^-C^+ in Fig. 7). Finally, we demonstrated how our model generates these cellular phenotypes by the combined effects of two signaling pathways, one that signals to Myc and the other to a transcription factor that induces differentiation.

APPENDIX

Dimensionless forms of Eqs. 10–14

$$\frac{dm^*}{dt^*} = \frac{1}{k_1' + s_2' p^*} - m^*, \tag{A1}$$

$$\delta' \frac{dp^*}{dt^*} = k_2' m^* + k_{14}' q^* + \frac{1}{k_3' + s_1' m^* + s_4' w^*} - p^*, \tag{A2}$$

$$\delta'' \frac{dw^*}{dt^*} = k_{16}' p^* + \frac{1}{k_{17}' + s_3' q^* + s_5' v^*} - w^*, \tag{A3}$$

$$\delta''' \frac{dq^*}{dt^*} = \varepsilon_3' + k_{13}' p^* - q^*, \tag{A4}$$

$$\delta'''' \frac{dv^*}{dt^*} = \varepsilon_5' + \frac{k_{15}' m^*}{k_{19}' + p^*} - v^*, \tag{A5}$$

where

$$t^* = \delta_m t,\ m^* = \frac{m}{s_1},\ p^* = \frac{p}{s_2},\quad q^* = \frac{q}{s_3},\ w^* = \frac{w}{s_4},\ v^* = \frac{v}{s_5}, \tag{A6}$$

$$\delta' = \frac{\delta_m}{\delta_p},\ \delta'' = \frac{\delta_m}{\delta_w},\ \delta''' = \frac{\delta_m}{\delta_q},\quad \delta'''' = \frac{\delta_m}{\delta_v},\ \varepsilon_3' = \frac{\varepsilon_3}{\delta_q},\ \varepsilon_5' = \frac{\varepsilon_5}{\delta_v}, \tag{A7}$$

$$s_1' = \frac{\delta_p}{\varepsilon_2} s_1,\ s_2' = \frac{\delta_m}{\varepsilon_1} s_2,\ s_3' = \frac{\delta_w}{\varepsilon_4} s_3,\quad s_4' = \frac{\delta_p k_{12}}{\varepsilon_2} s_4,\ s_5' = \frac{\delta_w k_{18}}{\varepsilon_4} s_5, \tag{A8}$$

$$k_1' = \frac{\delta_m}{\varepsilon_1} k_1,\ k_2' = \frac{s_1}{s_2 \delta_p} k_2,\quad k_3' = \frac{\delta_p}{\varepsilon_2} k_3,\ k_{13}' = \frac{s_2}{\delta_q s_3} k_{13}, \tag{A9}$$

$$k_{14}' = \frac{s_3}{s_2 \delta_p} k_{14},\ k_{15}' = \frac{s_1}{s_2 s_5 \delta_v} k_{15},\quad k_{16}' = \frac{s_2}{\delta_w s_4} k_{16},\ k_{17}' = \frac{\delta_w}{\varepsilon_4} k_{17},\ k_{19}' = \frac{k_{19}}{s_2}. \tag{A10}$$

Dimensionless forms of Eqs. 15–18

$$\delta_{ms}' \frac{dD_s^*}{dt^*} = s_s' + \frac{\left(k_6' + k_{6b}' m^*\right) D_s^{*4}}{1 + D_s^{*4} + k_5' p^* + k_{5b}' D_d^*} - D_s^*, \tag{A11}$$

$$\delta_{md}' \frac{dD_d^*}{dt^*} = s_d' + \frac{\left(k_7' + k_{7b}' p^*\right) D_d^{*4}}{1 + D_d^{*4} + k_4' m^* + k_{4b}' D_s^*} - D_d^*, \tag{A12}$$

$$\delta_{mc}' \frac{dP_c^*}{dt^*} = s_c' + \frac{\left(k_8' + k_{8b}' m^*\right) P_c^{*2}}{1 + P_c^{*2} + k_{11}' p^*} - P_c^*, \tag{A13}$$

$$\delta_{ma}' \frac{dP_a^*}{dt^*} = s_a' + \frac{\left(k_{10}' + k_{10b}' m^* + k_9' p^*\right) P_a^{*2}}{1 + P_a^{*2}} - P_a^*, \tag{A14}$$

where

$$t^* = \delta_m t,\ m^* = \frac{m}{s_1},\ p^* = \frac{p}{s_2},$$
$$D_s^* = \frac{D_s}{\theta_s},\ D_d^* = \frac{D_d}{\theta_d},\ P_c^* = \frac{P_c}{\theta_c},\ P_a^* = \frac{P_a}{\theta_a}, \tag{A15}$$

$$k_1' = \frac{\delta_m}{\varepsilon_1}k_1,\ k_2' = \frac{s_1}{s_2\delta_p}k_2,\ k_3' = \frac{\delta_p}{\varepsilon_2}k_3,$$
$$k_5' = \frac{s_2}{\theta_s^4}k_5,\ k_6' = \frac{1}{\theta_s\delta_s}k_6,\ k_{6b}' = \frac{S_1}{\theta_s\delta_s}k_{6b}, \tag{A16}$$

$$k_{5b}' = \frac{\theta_d}{\theta_s^4}k_5,\ k_7' = \frac{1}{\theta_d\delta_d}k_7,\ k_{7b}' = \frac{s_2}{\theta_d\delta_d}k_{7b},$$
$$k_4' = \frac{s_1}{\theta_d^4}k_4,\ k_{4b}' = \frac{\theta_s}{\theta_d^4}k_{4b},\ k_8' = \frac{1}{\theta_c\delta_c}k_8, \tag{A17}$$

$$k_{8b}' = \frac{s_1}{\theta_c\delta_c}k_{8b},\ k_{11}' = \frac{s_2}{\theta_c^2}k_{11},$$
$$k_{10}' = \frac{1}{\theta_a\delta_a}k_{10},\ k_{10b}' = \frac{s_1}{\theta_a\delta_a}k_{10b},\ k_9' = \frac{s_2}{\theta_a\delta_a}k_9, \tag{A18}$$

$$s_1' = \frac{\delta_p}{\varepsilon_2}s_1,\ s_2' = \frac{\delta_m}{\varepsilon_1}s_2,\ s_s' = \frac{\varepsilon_s}{\theta_s\delta_s}s_s,$$
$$s_d' = \frac{\varepsilon_d}{\theta_d\delta_d}s_d,\ s_c' = \frac{\varepsilon_c}{\theta_c\delta_c}s_c,\ s_a' = \frac{\varepsilon_a}{\theta_a\delta_a}s_a, \tag{A19}$$

$$\delta' = \frac{\delta_m}{\delta_p},\ \delta_{\mathrm{ms}}' = \frac{\delta_m}{\delta_s},\ \delta_{\mathrm{md}}' = \frac{\delta_m}{\delta_d},$$
$$\delta_{\mathrm{mc}}' = \frac{\delta_m}{\delta_c},\ \delta_{\mathrm{ma}}' = \frac{\delta_m}{\delta_a}. \tag{A20}$$

SUPPORTING MATERIAL

Two additional parts with one table and supporting equations are available at http://www.biophysj.org/biophysj/supplemental/S0006-3495(11)01183-0.

Funding was provided by the Intramural Research Program of the National Institutes of Health, National Cancer Institute. Y.K. was supported by a Faculty Research Grant from the University of Michigan-Dearborn.

REFERENCES

1. Rochlitz, C. F., I. Heide, …, E. de Kant. 1995. Evidence for a mutual regulation of p53 and c-Myc expression in human colorectal cancer metastases. *Ann. Oncol.* 6:981–986.
2. Nagao, M., K. Campbell, …, M. Nakafuku. 2008. Coordinated control of self-renewal and differentiation of neural stem cells by Myc and the p19ARF-p53 pathway. *J. Cell Biol.* 183:1243–1257.
3. Clevers, H. 2011. The cancer stem cell: premises, promises and challenges. *Nat. Med.* 17:313–319.
4. Pérez Castillo, A., D. Aguilar-Morante, …, J. Dorado. 2008. Cancer stem cells and brain tumors. *Clin. Transl. Oncol.* 10:262–267.
5. Tan, B. T., C. Y. Park, …, I. L. Weissman. 2006. The cancer stem cell hypothesis: a work in progress. *Lab. Invest.* 86:1203–1207.
6. Dalerba, P., R. W. Cho, and M. F. Clarke. 2007. Cancer stem cells: models and concepts. *Annu. Rev. Med.* 58:267–284.
7. Zheng, H., H. Ying, …, R. A. DePinho. 2008. p53 and Pten control neural and glioma stem/progenitor cell renewal and differentiation. *Nature.* 455:1129–1133.
8. Jacques, T. S., A. Swales, …, S. Brandner. 2010. Combinations of genetic mutations in the adult neural stem cell compartment determine brain tumor phenotypes. *EMBO J.* 29:222–235.
9. Chow, L. M., R. Endersby, …, S. J. Baker. 2011. Cooperativity within and among Pten, p53, and Rb pathways induces high-grade astrocytoma in adult brain. *Cancer Cell.* 19:305–316.
10. Aguda, B. D., and A. B. Goryachev. 2007. From pathways databases to network models of switching behavior. *PLOS Comput. Biol.* 3:1674–1678.
11. Boyer, L. A., T. I. Lee, …, R. A. Young. 2005. Core transcriptional regulatory circuitry in human embryonic stem cells. *Cell.* 122: 947–956.
12. Chen, X., V. B. Vega, and H. H. Ng. 2008. Transcriptional regulatory networks in embryonic stem cells. *Cold Spring Harb. Symp. Quant. Biol.* 73:203–209.
13. Chickarmane, V., and C. Peterson. 2008. A computational model for understanding stem cell, trophectoderm and endoderm lineage determination. *PLoS ONE.* 3:e3478.
14. Aguda, B. D., and C. K. Algar. 2003. A structural analysis of the qualitative networks regulating the cell cycle and apoptosis. *Cell Cycle.* 2:538–544.
15. Craciun, G., B. Aguda, and A. Friedman. 2005. Mathematical analysis of a modular network coordinating the cell cycle and apoptosis. *Math. Biosci. Eng.* 2:473–485.
16. Glauche, I., M. Herberg, and I. Roeder. 2010. Nanog variability and pluripotency regulation of embryonic stem cells—insights from a mathematical model analysis. *PLoS ONE.* 5:e11238.
17. MacArthur, B. D., C. P. Please, and R. O. Oreffo. 2008. Stochasticity and the molecular mechanisms of induced pluripotency. *PLoS ONE.* 3:e3086.
18. Aguda, B. D., Y. Kim, …, C. B. Marsh. 2008. MicroRNA regulation of a cancer network: consequences of the feedback loops involving miR-17-92, E2F, and Myc. *Proc. Natl. Acad. Sci. USA.* 105:19678–19683.
19. Murphy, D. J., M. R. Junttila, …, G. I. Evan. 2008. Distinct thresholds govern Myc's biological output in vivo. *Cancer Cell.* 14:447–457.
20. Grzmil, M., and B. A. Hemmings. 2010. Deregulated signaling networks in human brain tumors. *Biochim. Biophys. Acta.* 1804: 476–483.
21. Gregory, M. A., and S. R. Hann. 2000. c-Myc proteolysis by the ubiquitin-proteasome pathway: stabilization of c-Myc in Burkitt's lymphoma cells. *Mol. Cell. Biol.* 20:2423–2435.
22. Oren, M., W. Maltzman, and A. J. Levine. 1981. Post-translational regulation of the 54K cellular tumor antigen in normal and transformed cells. *Mol. Cell. Biol.* 1:101–110.
23. Olson, D. C., V. Marechal, …, A. J. Levine. 1993. Identification and characterization of multiple Mdm-2 proteins and Mdm-2-p53 protein complexes. *Oncogene.* 8:2353–2360.
24. Wu, X., K. Hepner, …, Y. E. Whang. 2000. Evidence for regulation of the PTEN tumor suppressor by a membrane-localized multi-PDZ domain containing scaffold protein MAGI-2. *Proc. Natl. Acad. Sci. USA.* 97:4233–4238.
25. Kuo, M. L., W. den Besten, …, C. J. Sherr. 2004. N-terminal polyubiquitination and degradation of the Arf tumor suppressor. *Genes Dev.* 18:1862–1874.
26. Ohgaki, H., P. Dessen, …, P. Kleihues. 2004. Genetic pathways to glioblastoma: a population-based study. *Cancer Res.* 64:6892–6899.
27. Ohgaki, H., and P. Kleihues. 2007. Genetic pathways to primary and secondary glioblastoma. *Am. J. Pathol.* 170:1445–1453.

28. Endersby, R., and S. J. Baker. 2008. PTEN signaling in brain: neuropathology and tumorigenesis. *Oncogene.* 27:5416–5430.

29. Koul, D. 2008. PTEN signaling pathways in glioblastoma. *Cancer Biol. Ther.* 7:1321–1325.

30. Mayo, L. D., and D. B. Donner. 2002. The PTEN, Mdm2, p53 tumor suppressor-oncoprotein network. *Trends Biochem. Sci.* 27:462–467.

31. Wee, K. B., and B. D. Aguda. 2006. Akt versus p53 in a network of oncogenes and tumor suppressor genes regulating cell survival and death. *Biophys. J.* 91:857–865.

32. Eitel, J. A., K. Bijangi-Vishehsaraei, …, L. D. Mayo. 2009. PTEN and p53 are required for hypoxia induced expression of maspin in glioblastoma cells. *Cell Cycle.* 8:896–901.

33. Wee, K. B., U. Surana, and B. D. Aguda. 2009. Oscillations of the p53-Akt network: implications on cell survival and death. *PLoS ONE.* 4:e4407.

34. Mayo, L. D., J. E. Dixon, …, D. B. Donner. 2002. PTEN protects p53 from Mdm2 and sensitizes cancer cells to chemotherapy. *J. Biol. Chem.* 277:5484–5489.

35. Trotman, L. C., and P. P. Pandolfi. 2003. PTEN and p53: who will get the upper hand? *Cancer Cell.* 3:97–99.

36. Freeman, D. J., A. G. Li, …, H. Wu. 2003. PTEN tumor suppressor regulates p53 protein levels and activity through phosphatase-dependent and -independent mechanisms. *Cancer Cell.* 3:117–130.

37. Biernat, W., P. Kleihues, …, H. Ohgaki. 1997. Amplification and overexpression of MDM2 in primary (de novo) glioblastomas. *J. Neuropathol. Exp. Neurol.* 56:180–185.

38. Marine, J. C., and G. Lozano. 2010. Mdm2-mediated ubiquitylation: p53 and beyond. *Cell Death Differ.* 17:93–102.

39. Lu, X. 2010. Tied up in loops: positive and negative autoregulation of p53. *Cold Spring Harb. Perspect. Biol.* 2:a000984.

40. Uhrbom, L., C. Dai, …, E. C. Holland. 2002. Ink4a-Arf loss cooperates with KRas activation in astrocytes and neural progenitors to generate glioblastomas of various morphologies depending on activated Akt. *Cancer Res.* 62:5551–5558.

41. Robinson, J. P., M. W. Vanbrocklin, …, S. L. Holmen. 2011. Activated MEK cooperates with Ink4a/Arf loss or Akt activation to induce gliomas in vivo. *Oncogene.* 30:1341–1350.

42. Zindy, F., C. M. Eischen, …, M. F. Roussel. 1998. Myc signaling via the ARF tumor suppressor regulates p53-dependent apoptosis and immortalization. *Genes Dev.* 12:2424–2433.

43. Eischen, C. M., J. D. Weber, …, J. L. Cleveland. 1999. Disruption of the ARF-Mdm2-p53 tumor suppressor pathway in Myc-induced lymphomagenesis. *Genes Dev.* 13:2658–2669.

44. Jin, S., and A. J. Levine. 2001. The p53 functional circuit. *J. Cell Sci.* 114:4139–4140.

45. Lev Bar-Or, R., R. Maya, …, M. Oren. 2000. Generation of oscillations by the p53-Mdm2 feedback loop: a theoretical and experimental study. *Proc. Natl. Acad. Sci. USA.* 97:11250–11255.

46. Cartwright, P., C. McLean, …, S. Dalton. 2005. LIF/STAT3 controls ES cell self-renewal and pluripotency by a Myc-dependent mechanism. *Development.* 132:885–896.

47. Katoh, M. 2008. WNT signaling in stem cell biology and regenerative medicine. *Curr. Drug Targets.* 9:565–570.

48. Cowling, V. H., and M. D. Cole. 2007. Turning the tables: Myc activates Wnt in breast cancer. *Cell Cycle.* 6:2625–2627.

49. Fujikura, J., E. Yamato, …, H. Niwa. 2002. Differentiation of embryonic stem cells is induced by GATA factors. *Genes Dev.* 16:784–789.

50. Smith, K. N., A. M. Singh, and S. Dalton. 2010. Myc represses primitive endoderm differentiation in pluripotent stem cells. *Cell Stem Cell.* 7:343–354.

51. Hough, S. R., I. Clements, …, K. A. Wiederholt. 2006. Differentiation of mouse embryonic stem cells after RNA interference-mediated silencing of OCT4 and Nanog. *Stem Cells.* 24:1467–1475.

52. Futreal, P. A., L. Coin, …, M. R. Stratton. 2004. A census of human cancer genes. *Nat. Rev. Cancer.* 4:177–183.

53. Santarius, T., J. Shipley, …, C. S. Cooper. 2010. A census of amplified and overexpressed human cancer genes. *Nat. Rev. Cancer.* 10:59–64.

54. Kim, J., J. H. Lee, and V. R. Iyer. 2008. Global identification of Myc target genes reveals its direct role in mitochondrial biogenesis and its E-box usage in vivo. *PLoS ONE.* 3:e1798.

55. Fernandez, P. C., S. R. Frank, …, B. Amati. 2003. Genomic targets of the human c-Myc protein. *Genes Dev.* 17:1115–1129.

56. Wang, L., Q. Wu, …, S. Liu. 2001. Analyses of p53 target genes in the human genome by bioinformatic and microarray approaches. *J. Biol. Chem.* 276:43604–43610.

57. Mirza, A., Q. Wu, …, S. Liu. 2003. Global transcriptional program of p53 target genes during the process of apoptosis and cell cycle progression. *Oncogene.* 22:3645–3654.